Check for updates

ADVANCING EARTH AND SPACE SCIENCES

Geophysical Research Letters

RESEARCH LETTER
10.1029/2025GL114775

On Risk of Rain on Snow Over High-Latitude Coastal Areas in North America

Azharuddin Mohammed[1], **Ardeshir Ebtehaj**[1], **Judah Cohen**[2], **and Efi Foufoula-Georgiou**[3]

[1]Saint Anthony Falls Laboratory, Department of Civil, Environmental and Geo-Engineering, University of Minnesota, Minneapolis, MN, USA, [2]Atmospheric & Environmental Research, Massachusetts Institute of Technology, Cambridge, MA, USA, [3]Department of Civil and Environmental Engineering, University of California, Irvine, CA, USA

Key Points:

- The climatology of rain-on-snow (ROS) events is presented by normalizing ROS instances with the snowpack duration
- High-altitude mountainous watersheds and high-latitude coastal regions are at an elevated ROS risk in North America
- Trends in rainfall excess and snowmelt in south central Alaska, the Olympic Mountains, and the Sierra Nevada highlight rising ROS flood risk

Supporting Information:

Supporting Information may be found in the online version of this article.

Correspondence to:

A. Ebtehaj,
ebtehaj@umn.edu

Citation:

Mohammed, A., Ebtehaj, A., Cohen, J., & Foufoula-Georgiou, E. (2025). On risk of rain on snow over high-latitude coastal areas in North America. *Geophysical Research Letters*, *52*, e2025GL114775. https://doi.org/10.1029/2025GL114775

Received 8 JAN 2025
Accepted 12 APR 2025

Author Contributions:

Conceptualization: Ardeshir Ebtehaj
Data curation: Azharuddin Mohammed
Formal analysis: Azharuddin Mohammed, Ardeshir Ebtehaj
Funding acquisition: Ardeshir Ebtehaj, Judah Cohen
Investigation: Azharuddin Mohammed, Ardeshir Ebtehaj
Methodology: Azharuddin Mohammed, Ardeshir Ebtehaj
Resources: Ardeshir Ebtehaj
Software: Azharuddin Mohammed
Supervision: Ardeshir Ebtehaj
Validation: Azharuddin Mohammed, Ardeshir Ebtehaj
Visualization: Azharuddin Mohammed
Writing – original draft: Azharuddin Mohammed, Ardeshir Ebtehaj

Abstract Extreme floods and landslides in high-latitude watersheds have been associated with rain-on-snow (ROS) events. Yet, the risks of changing precipitation phases on a declining snowpack under a warming climate remain unclear. Normalizing the total annual duration of ROS with that of the seasonal snowpack, the ERA5 data (1941–2023) show that the frequency of high-runoff ROS events is a characteristic feature of high-latitude coastal zones, particularly over the coasts of south-central Alaska and southern Newfoundland. Total rainfall accumulation per seasonal snowpack duration has increased across western mountain ranges, with the Olympic Mountains experiencing more than 40 mm of additional rainfall over the snowpack in the past eight decades, followed by the Sierra Nevada. These trends could drive an 8% increase in rainfall extremes (e.g., more than 10 mm for 6 hr storm with a 15-year return period), highlighting the need for resilient flood control systems in high-latitude coastal cities.

Plain Language Summary Rain-on-snow (ROS) events have caused flooding, including the 2013 Alberta floods and the 2017 California floods in the northern Sierra Nevada. As global warming accelerates, more precipitation falls as rain rather than snow, particularly in regions with historically persistent snowpack. Our analysis of flood-producing ROS events across North America indicates that the risk of ROS flooding is lower in historically snow-covered interior lowlands of the central United States than in high-altitude mountainous watersheds and high-latitude coastal regions. We present risk maps for various rainfall return periods and durations to support understanding the risks of coastal ROS-driven floods in a warming world.

1. Introduction

The problem of rain-on-snow (ROS) brings to bear critical questions closely tied to our era as rising global temperatures reshape the spatiotemporal dynamics of precipitation and snowpack. With increasing global temperatures, a growing proportion of precipitation is occurring as rain rather than snow (Klos et al., 2014; Ombadi et al., 2023; Tamang et al., 2020), leading to a continued reduction in the extent and duration of snowpack across the Northern Hemisphere (NH) (Gottlieb & Mankin, 2024; Matiu & Hanzer, 2022). These changes will affect the intensity, duration, and space-time frequency of ROS events and consequent potential floodings (López-Moreno et al., 2021; Myers et al., 2023; Sobota et al., 2020). Catastrophic floods have already been linked to heavy rainfall during snowmelt seasons, such as the 2013 historical Alberta floods (Pomeroy et al., 2016) and the one that coincided with California's 2017 Oroville Dam failure (Henn et al., 2020; Michaelis et al., 2022). More recently, springtime widespread flooding across the Midwest (Velásquez et al., 2023), frequent coastal landslides (Smith & Wegmann, 2018) in Western Contiguous United States (CONUS) and southeast Alaska (Bieniek et al., 2018; Pan et al., 2018) urges the necessity of expanding our understanding of the regional trends in characteristics of ROS events and their nonstationary impacts on spring flooding across North America.

The spatial distribution of ROS and its long-term trends are shaped by the interplay of precipitation amount, phase transitions, and snow-cover persistence, all of which are strongly influenced by air temperature and regional topography. On the one hand, a warming climate reduces the duration and extent of snow cover, decreasing the likelihood of ROS events and extreme runoff in lowland areas (Bonsoms et al., 2024; Rasiya Koya et al., 2024). On the other hand, increased rainfall (Prein & Heymsfield, 2020) heightens the probability of ROS events over persistent high-altitude snowpack (Li et al., 2019). Significant ROS events have been documented in high-altitude mountainous watersheds, including the Cascade Range and the Rockies in the west (McCabe et al., 2007), as well as the Appalachians and its highland subranges in the east (Pradhanang et al., 2013; Rasiya Koya et al., 2024),

Writing – review & editing: Azharuddin Mohammed, Ardeshir Ebtehaj, Judah Cohen, Efi Foufoula-Georgiou

with potential impacts on spring flooding (Graybeal & Leathers, 2006; Huang et al., 2022). Evidence also suggests that the climate of high-latitude coastal regions is transitioning more to a temperate environment (Evan & Eisenman, 2021; Zaqout & Andradóttir, 2024) due to a continuous rise of air temperature, giving rise to a more significant likelihood of ROS events over persistent, deep, and wet maritime snowpack (Il Jeong & Sushama, 2018).

Despite scientific consensus about the importance of ROS events in current and future scenarios of spring flooding over historically snow-dominated watersheds and coastal regions (Beniston & Stoffel, 2016; Morán-Tejeda et al., 2016; Musselman et al., 2018; Notarnicola, 2020; Stoelinga et al., 2010; Ye et al., 2008), it is not well understood how the competing dynamics of precipitation phase change and snowpack decline contribute to the ROS multi-decadal trends across North America. More importantly, the risks associated with ROS runoff remain poorly understood, particularly under non-stationary conditions driven by changes in rainfall and snow cover characteristics. This knowledge gap is especially pronounced across coastal mountain ranges in the Eastern United States, Alaska, and Canada, where snowpack telemetry and precipitation gauge stations are either absent or extremely sparse (Brunet & Milbrandt, 2023).

Given the declining snowpack trends in most of the continent (Mote et al., 2018; Siirila-Woodburn et al., 2021), unlike previous works, this study normalizes the total hourly counts of ROS events by the snowpack duration (NROS) to gain new regional insights into the multi-decadal trends in the frequency and amount of ROS events per snowpack duration. To that end, data from the fifth generation of the European Center for Medium-Range. Weather Forecasts atmospheric reanalysis (ERA5, Hersbach et al., 2020) are used and cross-validated with in situ observations. Similar to previous studies (Musselman et al., 2018), we focus on high runoff ROS events where and when the rainfall rate and the snow water equivalent (SWE) are greater than 2 mm hr^{-1} and 10 mm, respectively, and the snowmelt comprises at least 10% of total rainfall excess (i.e., amount of rainfall available for overland surface runoff) and snowmelt flux—consistent with several previous literature (Colle & Mass, 2000; Kattelmann et al., 1991; Li et al., 2019; Musselman et al., 2018). Hereafter, this snowpack condition is denoted by SWE_{10}, and the terms rainfall and rainfall excess are used interchangeably. The trends over mountain ranges and non-stationarity of the intensity-duration-frequency (IDF) of ROS events are also studied, highlighting the need for efforts in assessing the risk of ROS runoff for future infrastructure developments in regions of high vulnerability. We need to mention that throughout, the concept of "risk" is used in the context of classic rainfall frequency analysis (Stedinger et al., 1993) and its non-stationary projections (Cheng & AghaKouchak, 2014) without implicitly accounting for other factors that might affect individual events (e.g., antecedent soil moisture) and streamflow flooding.

2. Data and Methods

2.1. Data

Hourly ERA5 data for total near-surface precipitation (m), snowfall (m), snow depth (m), snowmelt flux (m), and snow density (kg m^{-3}) at 0.25° resolution from 1941 to 2023, are utilized to identify ROS events and their normalized representation. The computed NROS annual trends are validated against gauge data from the Global Historical Climatology Network Daily (GHCNd, Menne et al., 2012) dataset, which contains the required key variables, including total precipitation, snowfall, and snow depth. Across North America, the GHCNd dataset offers measurements in more than 73,000 gauge stations, with fewer than 9,000 in Canada. Only those gauges with less than 10% missing values and at least 30 years of overlap with the reanalysis data were used. Total precipitation values larger than 400 mm were flagged as outliers. The GHCNd dataset includes quality flags (NCEI, 2024) indicating inconsistencies such as "temperature is too high for snow." Data marked by any of these inconsistency flags were excluded. Ultimately, 517 gauge stations were selected during the overlapping period 1980–2010 after quality control. A discussion of how the NROS is validated against the GHCNd observations is presented in Supporting Information S1. In addition to the above data, we utilized Global Multi-resolution Terrain Elevation Data 2010 by Danielson and Gesch (2011) to characterize dependencies with topography.

10.1029/2025GL114775

2.2. NROS Events

As is self-evident, ROS events are characterized not only by changes in the precipitation phase but also by the presence of snow cover, which are tightly dependent on each other over sufficiently long time scales. The annual NROS events are computed as follows:

$$NROS = \frac{|\mathrm{R}|}{|\mathrm{S}|}, \tag{1}$$

where the sets R and S are defined as $R = \{r \mid r > 2 \text{ mm h}^{-1}\}$ and $S = \{\text{SWE} \mid \text{SWE} > 10 \text{ mm}\}$ and $|\cdot|$ is the cardinality or size of the set, representing the total number of instances in a year when rainfall and SWE exceed their respective thresholds. As previously noted, the NROS events and computations are also confined only to events where and when the snowmelt comprises at least 10% of total runoff potential (Li et al., 2017) (i.e., the sum of excess rainfall and snowmelt flux).

Since GHCNd data lacks snow density measurements, for computation of NROS, we estimate SWE based on its relationship (Sturm et al., 2010) with snow depth for different snow classes (i.e., Tundra, Taiga, Maritime, Ephemeral, Prairie, and Alpine) as follows:

$$\rho_{h,DOY} = (\rho_{max} - \rho_{min})\,[1 - \exp(-k_1 \times h - k_2 \times \text{DOY})] + \rho_{min}, \tag{2}$$

where for a specific snow class, $\rho_{\max}$ and $\rho_{\min}$, in kg m^{-3}, represent the maximum and minimum snow densities, k_1 and k_2 are constant parameters, and h denotes snow depth in meters at day of the year (DOY).

2.3. ROS Runoff Trend Analysis

Analogously, for trend analyses, we normalize annual rainfall excess R_e and snowmelt flux R_s, in millimeters, by the SWE$_{10}$ snowpack duration to identify regions vulnerable to ROS-related risks. We use the non-parametric Theil—Sen estimator (Sen, 1968) for linear trend analysis. This approach obtains the median of the slopes, namely Sen's slope, of all lines connecting unique pairs of annual NROS representations. Compared to classic least squares, the method is robust to outliers, non-Gaussian, and heteroskedastic residuals (Matoušek et al., 1998; Wilcox, 2010). The Sen's slope is insensitive to outliers and provides robust estimates of linear trends. The statistical significance of these trends is evaluated using the Mann-Kendall test (Kendall, 1948; Mann, 1945). A trend is considered significant when the p-values are less than 0.05, assuming the null hypothesis follows a Gaussian distribution.

2.4. ROS Extreme Values

The extreme values of 1, 3, and 6 hr total ROS for 5, 10, and 15 years return periods are computed. We need to note that, while computing these extremes, the snowpack must persist for the required duration. To that end, the three-parameter Generalized Extreme Value (GEV) distribution is used with location μ, scale σ, and shape ξ parameters. To account for non-stationarity in the annual maximum time series, a linear trend $\mu(\beta_0, \beta_1) = \beta_0 + \beta_1 T$ is considered for the location parameter (Cheng & AghaKouchak, 2014) with $T = 83$. All unknown parameters of the distribution are obtained through the maximum likelihood approximation for the entire data set (Ruggiero et al., 2010). The extreme values of interest Z_{TR} for a return period of T_R are obtained as follows:

$$Z_{T_R} = \begin{cases} \hat{\mu} + \dfrac{\hat{\sigma}}{\hat{\xi}}\left[\left(-ln\left(1 - \dfrac{1}{T_R}\right)\right)^{-\hat{\xi}} - 1\right], & for\ \hat{\xi} \neq 0\ and\ \dfrac{1}{T_R} < 1 \\ \hat{\mu} + \hat{\sigma}\, ln\left(-ln\left(1 - \dfrac{1}{T_R}\right)\right), & for\ \hat{\xi} = 0\ and\ T_R > 1 \end{cases}, \tag{3}$$

where $\hat{\mu}(T_R) = \hat{\beta}_0 + \hat{\beta}_1\, T_R$, $\hat{\sigma}$, and $\hat{\xi}$ are the estimated parameters. Consequently, the extreme value estimates provide insights into future projections and risks, reflecting the increased probability of exceedance due to the shift in the mean of the fitted distributions.

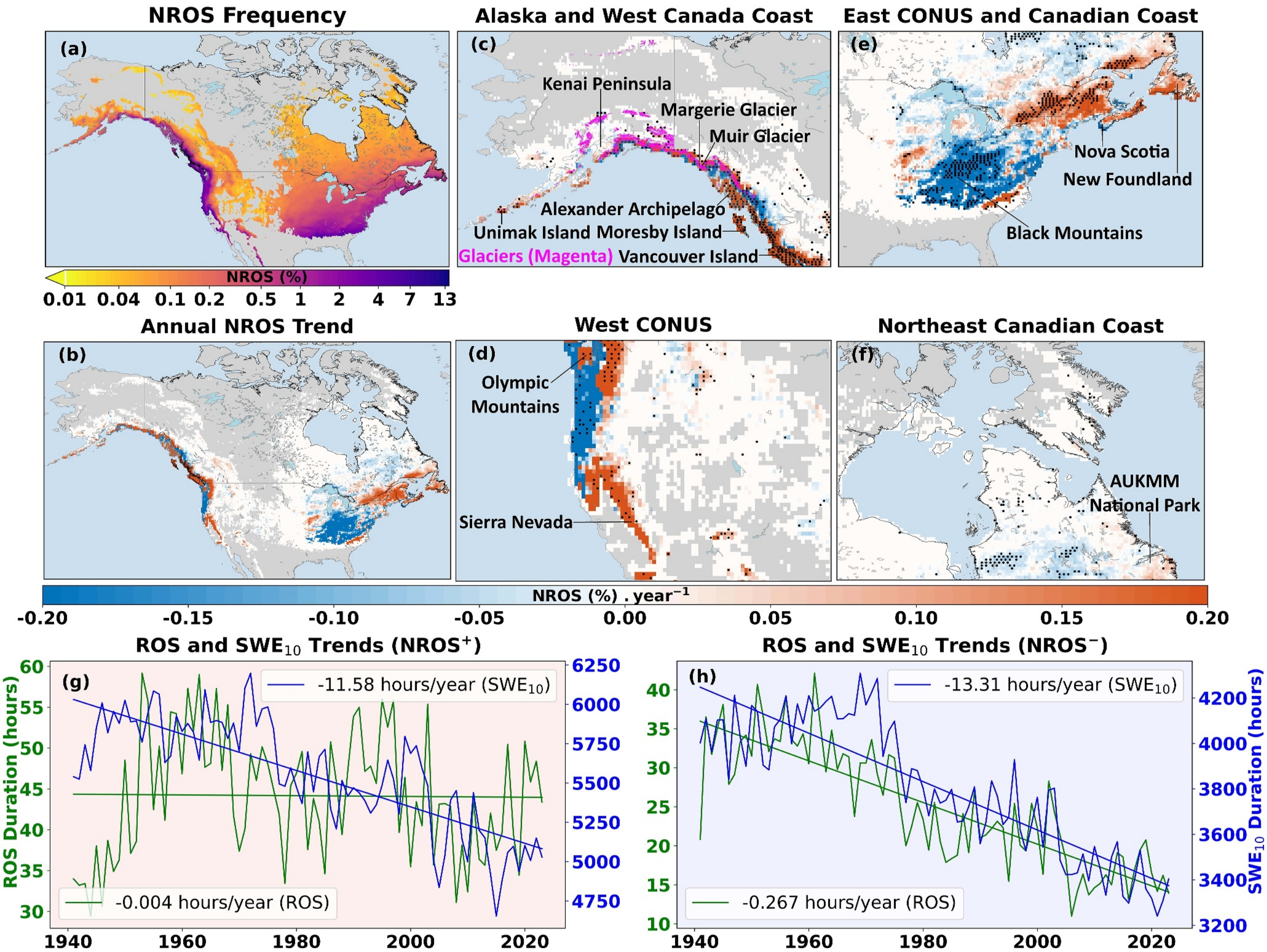

Figure 1. (a) Percentage of mean annual normalized ROS (NROS) frequency, (b) trends in annual NROS from 1941 to 2023, and (c)–(f) zoomed-in plots, along with annual time series of rain-on-snow and SWE_{10} durations for pixels with significantly, (g) positive ($NROS^+$), and (h) negative ($NROS^-$) trends. Significant trends ($p < 0.05$) are marked with black dots, and Alaskan glaciers' extent (Roberts-Pierel et al., 2022) is shown in magenta in panel c.

3. Results

3.1. NROS Climatology and Trends

The annual NROS frequency (Figure 1a) is notably higher along the coast than inland. In the west, the occurrence frequencies plainly show a latitudinal gradient, increasing from about 2% in southern Alaska to more than 10% along the coasts of Northern California and the Sierra Nevada, indicating the increased frequency of rainfall events over relatively longer duration SWE_{10} snowpack. Southeastern Alaska has isolated coastal areas with positive NROS frequencies (Bieniek et al., 2018) of around 5%, extending from the coasts of the Kenai Peninsula Borough and Chugach Mountains to the southeast Alaskan panhandle and the Alexander Archipelago. At lower latitudes, frequencies increase to more than 10% along the western slopes of the Coast Mountains in British Columbia, Vancouver Island, the Olympic Mountains in Washington State, and the Sierra Nevada in California.

In the Eastern part, the highest NROS frequencies of more than 5% are over a latitudinal band of ephemeral snow (Hatchett, 2021; Rahimi et al., 2022) stretching from northern Arkansas to the coasts of North Carolina. Along coastal areas, the relatively high NROS frequency of around 2% extends from the eastern slopes of the Green and White Mountains, across the coasts of Connecticut to New England, with higher rates over mountainous regions. Higher NROS frequencies over the Black Mountains in the Appalachians and Mount Mitchell in North Carolina further highlight the impact of topography on NROS events. In Canada, NROS with frequencies of around 2% are found in the Appalachian uplands of Nova Scotia, Avalon Peninsula, and southern Newfoundland and Labrador province, with higher values in the vicinity of coastlines. A detailed analysis of ROS and SWE_{10} frequencies is presented in Figure S1 in Supporting Information S1 to shed more light on the frequencies of the NROS's constituting elements.

The NROS annual trends show clusters of positive and negative values over the western and eastern parts of the continent (Figure 1b). Significant positive trends of around 2% per decade are observed over southern Alaska and the west coast of Canada, extending from the Unimak of the Aleutian Islands to Vancouver Island (Figure 1c). The Kenai Peninsula's coasts display a mixture of significant trends with different signs, leaning negative over the highlands of Kenai Fjords National Park. In the lower latitudes of southeast Alaska, a ribbon-like contrasting trend pattern emerges with positive values over the Alexander Archipelago lowlands and negative ones over the highlands of the Coast Range. Most southeast Alaskan glaciated coastal areas have experienced a positive trend encompassing regional glaciers such as the Margerie, Johns Hopkins, Brady, and Muir. The west coast of British Columbia exhibits widespread positive trends, particularly around Moresby and Vancouver Islands, indicating an increased risk of ROS events and potential coastal flooding. Past events have highlighted this risk, such as the widespread coastal flooding and landslides triggered by an atmospheric river on 14 November 2021, which caused loss of life and property (Gillett et al., 2022).

Significant positive trends are observed in lower latitudes in the western CONUS over the Olympic Mountains, Cascade Range, and Sierra Nevada (Figure 1d). In contrast, negative trends persist in the Coast Range of Washington and Oregon. The lowland Appalachian Mountains and their foothills have experienced declining trends in most parts, while positive trends are found across Maine, Newfoundland, and Nova Scotia highlands (Figure 1e). The decline of NROS in lowland Appalachians is because the snowpack exhibits a faster-declining rate than the increasing rate of precipitation phase transition from snow to rain. However, this pattern is reversed over Appalachian uplands, causing increased risks of high-latitude (i.e., approximately 60°N) ROS events. Trends across southeast Canada are less pronounced but still significant below 60°N, with positive values observed in the east over Akami-Uapishk^{u}-KakKasuak-Mealy Mountains (AUKMM) National Park Reserve in Newfoundland and Labrador, and negative values in the west, spanning central and southern Quebec province (Figure 1f).

The annual trends of ROS and SWE_{10} hourly durations are analyzed for the collection of all pixels with significantly positive ($NROS^{+}$) and negative ($NROS^{-}$) trends. Surprisingly, on one hand, in the regions with positive trends (Figure 1g), there is no significant trend in ROS duration, but a significant decline of 11.60 hr yr^{-1} in SWE duration is quantified. On the other hand, in the regions with negative trends (Figure 1h), both ROS and SWE durations show declines of 0.27 and 13.30 hr yr^{-1}, respectively. There are important findings here. The constant rate of ROS duration over a declining snowpack implies that the duration of rainfall events has increased at almost the same pace as the snowpack duration declined for regions with positive trends. In contrast, the snowpack has declined faster than any potential expansion of rainfall events in areas with negative trends. The spatial representation of annual trends of ROS and SWE durations is shown in Figure S1 in Supporting Information S1 for further insights.

As a function of elevation, the significant NROS and ROS trends are shown in Figure 2 together with the mean climatology of SWE_{10} duration. The NROS trends are continually positive and non-monotonic with elevation, capturing the competing effects of elevational changes in the precipitation phase and snowpack. On average, NROS has increased across North America, with the highest rates in altitudes 600–1,500 m, where SWE_{10} also experiences the most prolonged duration, corroborating the recent findings (Rasiya Koya et al., 2024). The NROS trends are almost negligible over landscapes with elevation above 2100 m. In contrast, ROS trends increase monotonically with elevation, showing negative (positive) trends below (above) 1,200–1,500 m. This contrasting picture underscores that although the frequency of ROS events has decreased in lowland areas due to the ongoing reduction of snowpack, the frequency of annual rainfall per snowpack duration has consistently and steadily increased over the past eight decades.

3.2. ROS Runoff Trends

To bring to light the reasons explaining changes in ROS potential runoff, it is imperative to untangle the impacts of its constituting elements: excess rainfall R_e and snowmelt flux R_s. The previously explained SWE_{10} condition is applied to confine our considerations to runoff potent ROS events. In the same vein, total magnitude of the annual

10.1029/2025GL114775

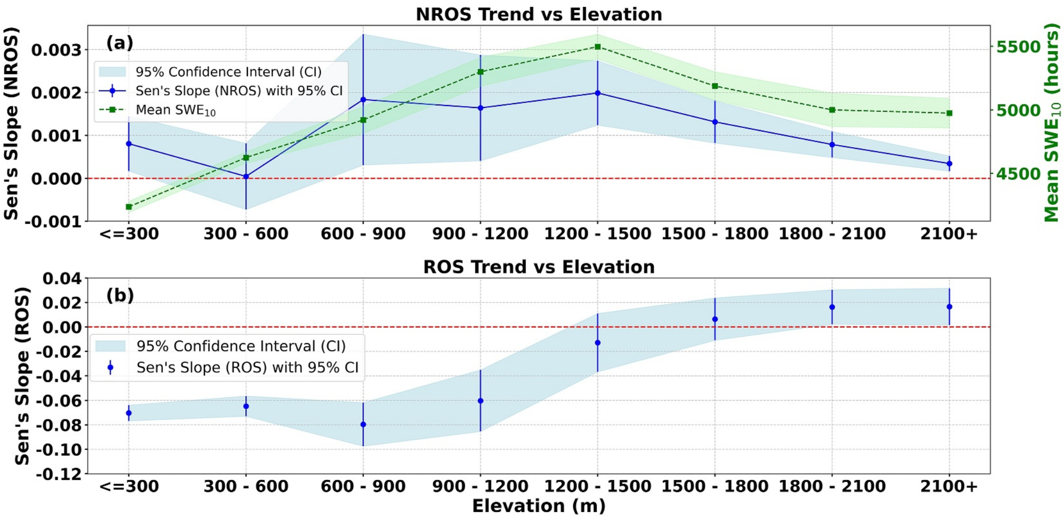

Figure 2. Elevation trends of (a) normalized ROS and mean SWE_{10}, and (b) rain-on-snow across North America, with 95% confidence bounds shown in shaded areas.

fluxes is normalized by the seasonal snowpack duration to uncover the trends independent of the declining snowpack.

The significant spatial trends in normalized R_e (Figure 3a) are consistent with those of NROS for the most part. Analogous to NROS trends, positive trends of 2 mm season^{-1} decade^{-1} of rainfall excess are notably observed over the Chugach region in southcentral Alaska. Surprisingly, this region exhibits notable positive trends in normalized snowmelt flux (Figure 3b) rarely observed elsewhere, marking it among the most vulnerable areas across the continent to the high risk of ROS runoff. Furthermore, unlike the NROS trend direction, the normalized excess rainfall over the Southeast Alaska Panhandle is declining. Therefore, the shrinking seasonal snowpack and

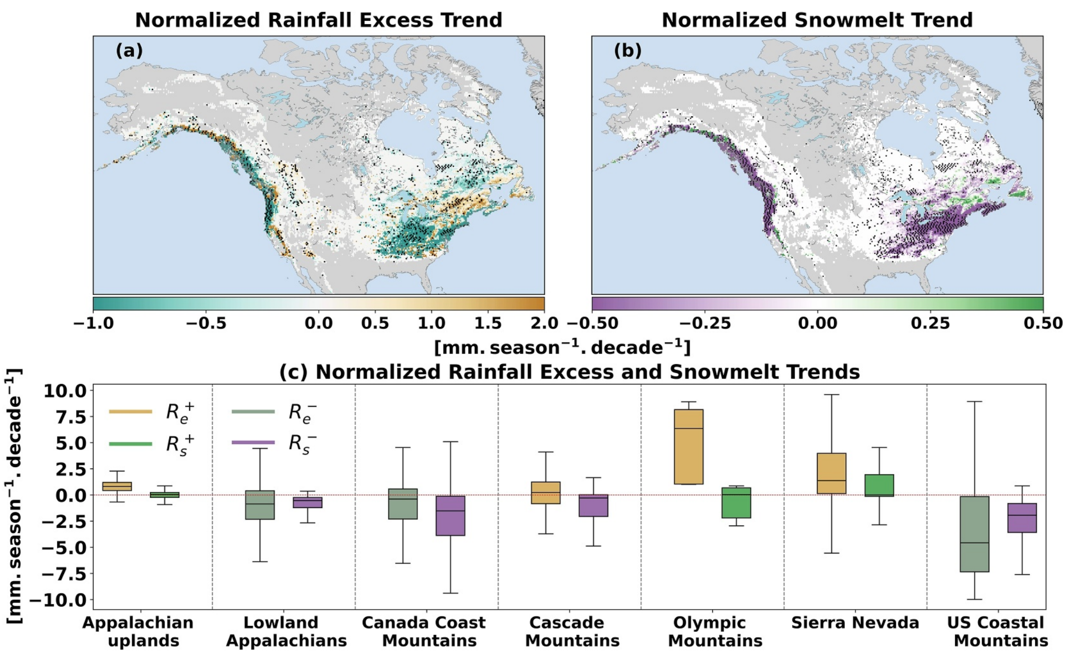

Figure 3. (a) Annual trend of normalized rainfall excess R_e, (b) normalized snowmelt R_s, and (c) box plots of their variability across major mountain ranges in North America. Significant trends ($p < 0.05$) are marked with black dots. In the box plot, the central mark represents the median, edges are the 25th and 75th percentiles, and whiskers extend to the most extreme data points. See Figure S3 in Supporting Information S1.

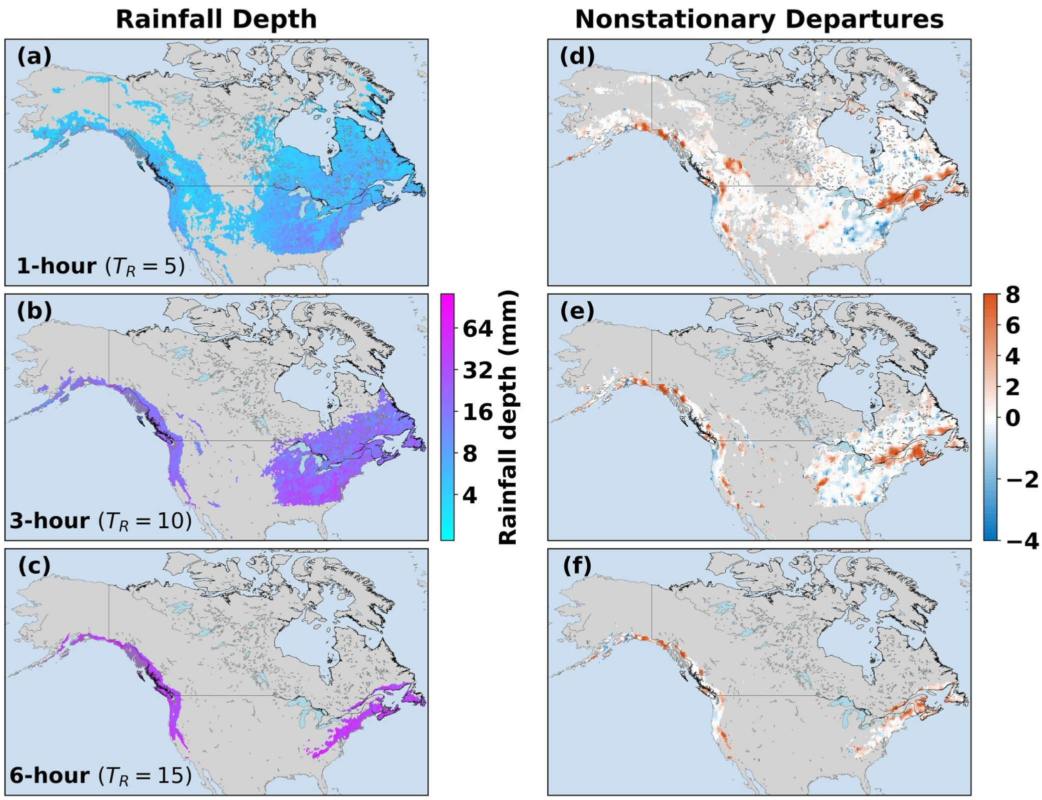

Figure 4. (a–c) Total 1, 3, and 6 hr rainfall excess for 5, 10, and 15 years return periods using a stationary generalized extreme value distribution, and (d–f) corresponding nonstationary departures. See the Method Section.

its flux seem to have outpaced any potential trend in precipitation phase change in this region. This continual reduction of annual excess rainfall extends to the Coast Range in Washington and Oregon, corroborating the NROS trends. Significant positive trends in excess rainfall and snowmelt fluxes over the Cascade Range, Olympic Mountains, Sierra Nevada, and northern Arizona further highlight the rising potential of ROS floods in these mountainous regions. Over the east, the patterns closely follow the pattern of NROS, indicating the frequency of ROS increases with latitude and becomes maximum in the northeast coasts of the United States and the southern coasts of Quebec and Newfoundland in Canada.

Statistical evaluation of the trends across different mountain ranges (see Figure S3 in Supporting Information S1) furnishes further clarity and a new regional and climatological understanding of the past changes. As shown in Figure 3c, the median trends of both fluxes show consistent signs across all mountain ranges, except over the Cascade Range. Our analysis indicated that (not shown here) over the Cascades, unlike other mountainous regions, the ROS snowmelt flux is decreasing faster than the decline in SWE_{10} duration. This declining trend in snowmelt makes sense as the increased amount of warm rain over the life cycle of the seasonal snowpack can accelerate melting due to the transfer of sensible heat from rain to snow in exchange for the latent heat of melting. The strongest positive trends and the widest uncertainty range are over the Olympic Mountains, followed by the Sierra Nevada. This can be attributed to the previous findings (Guan et al., 2016; Rhoades et al., 2024) suggesting the increased frequency of warm atmospheric rivers approaching the mountains of the west coasts. These concentrated bands of moisture plumes efficiently transport large amounts of water vapor from the tropics to the mid-latitudes in a relatively short period through strong low-level jets ahead of cold fronts that can dump a significant amount of rain over snow-covered surfaces.

3.3. ROS Extreme Values

A three-parameter GEV distribution is used to derive ROS depth for return periods of 5, 10, and 15 years with 1, 3, and 6 hr duration (Figure 4). The left panels show the extreme values with a stationary assumption. As explained in the Methods Section, the right panels display the percentages of changes when non-stationarity in the mean is accounted for. As the return period and ROS duration increase, extreme values become more pronounced, with their locations shifting from inland toward coastal zones, where high SWE snowpack persists.

The 1 hr ROS depth with a 5-year return period reaches 12 mm of total depth over a narrow band along the west coasts of the continent stretching from Alaska to Washington and a wide range of inland landscapes over the Midwest and East Coast. Flood-producing 6 hr ROS events with a return period of 15 years are chiefly coastal phenomena. Extreme 6 hr rainfall with a total depth of 64 mm can be found over Katmai and Lake Clark National Parks and Reserves in Southwest Alaska. These extremes stretch over southcentral Alaska, Kenai Fjord, Chugach National Forests, and the western flanks of the Elias Mountains in Southeast Alaska and Canada. As previously noted, the Olympic Mountains and the Sierra Nevada are the most vulnerable regions in the United States. The phenomenon is coastal mainly in the east, apart from the higher elevations in the Great Smoky Mountains and the Blue Ridge Mountains. The coastal areas of New Jersey and New York, the Nova Scotia Peninsula, and the southern coasts of the Canadian island of Newfoundland are vulnerable to this extreme ROS flooding.

4. Discussion and Concluding Remarks

Building on previous research (Cohen et al., 2015; Li et al., 2019; McCabe et al., 2007a; Musselman et al., 2018; Pradhanang et al., 2013; Wachowicz et al., 2020), using the ERA5 reanalysis hourly data in the past eight decades, the paper furnished new insights into the frequency of NROS events, the total annual amount of rainfall depth per snowpack seasonal duration, and its annual trends. While discrepancies were observed in comparisons with in situ data (see Supporting Information S1), the spatiotemporal direction of the trends was aligned. In particular, two distinct regional regimes emerged. The positive trends are where the snowfall-to-rainfall transition rates keep pace with the rate of snowpack decline. However, the declining snowpack rate outpaces the expansion rate of rainfall frequency in regions with negative NROS trends.

Consequently, the elevated risk of ROS flooding is diminishing over historically snow-covered interior lowlands in the central United States and shifting toward high-altitude mountainous watersheds and high-latitude coastal regions in Alaska, British Columbia, Quebec, Newfoundland, and Labrador. Amongst mountainous watersheds in North America, the Olympic Mountains, the Sierra Nevada, and the Appalachian uplands are the most vulnerable to increased frequency of ROS events. The anticipated impacts on coastal erosion (Nielsen et al., 2022), sediment dynamics (Moragoda & Cohen, 2020), streamflow hydrograph (Tohver et al., 2014), nutrient loads (Pihlainen et al., 2020), and phytoplankton blooms (Dai et al., 2023) underscore the need for future foundational studies that integrate the interconnected physical, chemical, and biological processes.

The observed positive NROS trends over Alaskan glaciers could trigger a self-reinforcing retreat feedback, highlighting the need for fundamental studies to explore the implications for regional ecohydrology and the socioeconomic development of local communities. Lastly, the non-stationary climate can increase the total amount of ROS by 8% (e.g., ~10 mm of more rain for a 6 hr storm with a return period of 15 years). The increased ROS events and amounts shall be accounted for when upgrading, designing, and managing the stormwater drainage systems in populated coastal cities in high-risk regions.

Conflict of Interest

The authors declare no conflicts of interest relevant to this study.

Data Availability Statement

ERA5 data (Hersbach et al., 2023) are available at the Copernicus Climate Change Service (C3S) Climate Data Store at https://cds.climate.copernicus.eu/#!/search?text=ERA5&type=dataset. The Global Historical Climatology Network-daily (GHCNd, Menne et al., 2012) data is publicly provided by the National Centers for Environmental Information (NCEI) at https://www.ncei.noaa.gov/products/land-based-station/global-historical-climatology-network-daily.

Acknowledgments

The funding support from NASA's Global Precipitation Measurement (PMM, 80NSSC22K0596) and the Legislative-Citizen Commission on Minnesota Resources (LCCMR, 2024-046) is greatly acknowledged. Judah Cohen acknowledges funding from the National Science Foundation (AGS-2140909). Efi Foufoula-Georgiou acknowledges support from NASA's Precipitation Measurement Mission (Grant 80NSSC22K0597) and the Weather and Atmospheric Dynamics program (Grant 80NSSC23K1304), as well as support of NSF's Division of Information and Intelligent Systems through the Expand AI2ES project (Grant IIS2324008) and the Samueli Endowed Chair.

References

Beniston, M., & Stoffel, M. (2016). Rain-on-snow events, floods and climate change in the Alps: Events may increase with warming up to 4°C and decrease thereafter. *Science of the Total Environment*, *571*, 228–236. https://doi.org/10.1016/j.scitotenv.2016.07.146

Bieniek, P. A., Bhatt, U. S., Walsh, J. E., Lader, R., Griffith, B., Roach, J. K., & Thoman, R. L. (2018). Assessment of Alaska rain-on-snow events using dynamical downscaling. *Journal of Applied Meteorology and Climatology*, *57*(8), 1847–1863. Retrieved from https://doi.org/10.1175/JAMC-D-17-0276.1

Bonsoms, J., López-Moreno, J. I., Alonso-González, E., Deschamps-Berger, C., & Oliva, M. (2024). Rain-on-snow responses to warmer Pyrenees: A sensitivity analysis using a physically based snow hydrological model. *Natural Hazards and Earth System Sciences*, *24*(1), 245–264. Retrieved from https://doi.org/10.5194/nhess-24-245-2024

Brunet, D., & Milbrandt, J. A. (2023). Optimal design of a surface precipitation network in Canada. *Journal of Hydrometeorology*. Retrieved from https://doi.org/10.1175/JHM-D-22-0085.1

Cheng, L., & AghaKouchak, A. (2014). Nonstationary precipitation intensity- duration-frequency curves for infrastructure design in a changing climate. *Scientific Reports*, *4*(1), 7093. https://doi.org/10.1038/srep07093

Cohen, J., Ye, H., & Jones, J. (2015). Trends and variability in rain-on-snow events. *Geophysical Research Letters*, *42*(17), 7115–7122. https://doi.org/10.1002/2015GL065320

Colle, B. A., & Mass, C. F. (2000). The 5–9 February 1996 flooding event over the Pacific Northwest: Sensitivity studies and evaluation of the MM5 precipitation Forecasts. *Monthly Weather Review*, *128*(3), 593–617. Retrieved from https://doi.org/10.1175/1520-0493(2000)128<0593:tffeot>2.0.co;2

Dai, Y., Yang, S., Zhao, D., Hu, C., Xu, W., Anderson, D. M., et al. (2023). Coastal phytoplankton blooms expand and intensify in the 21st century. *Nature*, *615*(7951), 280–284. Retrieved from https://doi.org/10.1038/s41586-023-05760-y

Danielson, J., & Gesch, D. (2011). *Global multi-resolution terrain elevation data 2010 (gmted2010) (Open-File Report No. 2011-1073)*. U.S. Geological Survey. Retrieved from https://pubs.usgs.gov/of/2011/1073/

Evan, A., & Eisenman, I. (2021). A mechanism for regional variations in snowpack melt under rising temperature. *Nature Climate Change*, *11*(4), 326–330. Retrieved from https://doi.org/10.1038/s41558-021-00996-w

Gillett, N. P., Cannon, A. J., Malinina, E., Schnorbus, M., Anslow, F., Sun, Q., et al. (2022). Human influence on the 2021 British Columbia floods. *Weather and Climate Extremes*, *36*, 100441. Retrieved from https://doi.org/10.1016/j.wace.2022.100441

Gottlieb, A. R., & Mankin, J. S. (2024). Evidence of human influence on Northern Hemisphere snow loss. *Nature*, *625*(7994), 293–300. https://doi.org/10.1038/s41586-023-06794-y

Graybeal, D. Y., & Leathers, D. J. (2006). Snowmelt-related flood risk in Appalachia: First estimates from a historical snow climatology. *Journal of Applied Meteorology and Climatology*, *45*(1), 178–193. Retrieved from https://doi.org/10.1175/JAM2330.1

Guan, B., Waliser, D. E., Ralph, F. M., Fetzer, E. J., & Neiman, P. J. (2016). Hydrometeorological characteristics of rain-on-snow events associated with atmospheric rivers. *Geophysical Research Letters*, *43*(6), 2964–2973. Retrieved from https://doi.org/10.1002/2016GL067978

Hatchett, B. J. (2021). Seasonal and ephemeral snowpacks of the conterminous United States. *Hydrology*, *8*(1), 32. Retrieved from https://doi.org/10.3390/hydrology8010032

Henn, B., Musselman, K. N., Lestak, L., Ralph, F. M., & Molotch, N. P. (2020). Extreme runoff generation from atmospheric river driven snowmelt during the 2017 Oroville Dam incident. *Geophysical Research Letters*, *47*(14), e2020GL088189. Retrieved from https://doi.org/10.1029/2020GL088189

Hersbach, H., Bell, B., Berrisford, P., Biavati, G., Horányi, A., Muñoz Sabater, J., & Thépaut, J.-N. (2023). ERA5 hourly data on single levels from 1940 to present [Dataset]. *Copernicus Climate Change Service (C3S) Climate Data Store (CDS)*. https://doi.org/10.24381/cds.adbb2d47. Accessed 01 08 2024.

Hersbach, H., Bell, B., Berrisford, P., Hirahara, S., Horányi, A., Muñoz-Sabater, J., et al. (2020). The ERA5 global reanalysis. *Quarterly Journal of the Royal Meteorological Society*, *146*(730), 1999–2049. https://doi.org/10.1002/qj.3803

Huang, H., Fischella, M. R., Liu, Y., Ban, Z., Fayne, J. V., Li, D., et al. (2022). Changes in mechanisms and characteristics of western U.S. Floods over the last sixty years. *Geophysical Research Letters*, *49*(3), e2021GL097022. https://doi.org/10.1029/2021GL097022

Il Jeong, D., & Sushama, L. (2018). Rain-on-snow events over North America based on two Canadian regional climate models. *Climate Dynamics*, *50*(1), 303–316. Retrieved from https://doi.org/10.1007/s00382-017-3609-x

Kattelmann, R. C., Berg, N. H., & McGurk, B. J. (1991). A history of rain-on-snow floods in the Sierra Nevada. In *59th annual western snow conference*. Juneau, Alaska: Western Snow Conference. Retrieved from /bibliography/1991Kattelmann.pdf

Kendall, M. G. (1948). *Rank correlation methods* (pp. 140–141). Journal of the Institute of Actuaries.

Klos, P. Z., Link, T. E., & Abatzoglou, J. T. (2014). Extent of the rain-snow transition zone in the western U.S. under historic and projected climate. *Geophysical Research Letters*, *41*(13), 4560–4568. https://doi.org/10.1002/2014GL060500

Li, D., Lettenmaier, D. P., Margulis, S. A., & Andreadis, K. (2019). The role of rain-on-snow in flooding over the conterminous United States. *Water Resources Research*, *55*(11), 8492–8513. https://doi.org/10.1029/2019WR024950

Li, D., Wrzesien, M. L., Durand, M., Adam, J., & Lettenmaier, D. P. (2017). How much runoff originates as snow in the western United States, and how will that change in the future? *Geophysical Research Letters*, *44*(12), 6163–6172. https://doi.org/10.1002/2017GL073551

López-Moreno, J. I., Pomeroy, J. W., Morán-Tejeda, E., Revuelto, J., Navarro-Serrano, F. M., Vidaller, I., & Alonso-González, E. (2021). Changes in the frequency of global high mountain rain-on-snow events due to climate warming. *Environmental Research Letters*, *16*(9), 094021. https://doi.org/10.1088/1748-9326/ac0dde

Mann, H. B. (1945). Nonparametric tests against trend. *Econometrica*, *13*(3), 245–259. https://doi.org/10.2307/1907187

Matiu, M., & Hanzer, F. (2022). Bias adjustment and downscaling of snow cover fraction projections from regional climate models using remote sensing for the European Alps. *Hydrology and Earth System Sciences*, *26*(12), 3037–3054. https://doi.org/10.5194/hess-26-3037-2022

Matoušek, J., Mount, D. M., & Netanyahu, N. S. (1998). Efficient randomized algorithms for the repeated median line estimator. *Algorithmica*, *20*(2), 136–150. https://doi.org/10.1007/PL00009190

McCabe, G. J., Clark, M. P., & Hay, L. E. (2007). Rain-on-Snow events in the western United States. *Bulletin of the American Meteorological Society*, *88*(3), 319–328. https://doi.org/10.1175/BAMS-88-3-319

Menne, M. J., Durre, I., Korzeniewski, B., McNeill, S., Thomas, K., Yin, X., & Houston, T. G. (2012). Global historical climatology network - Daily (ghcn-daily) version 3 [Dataset]. NOAA National Climatic Data Center. Retrieved from https://doi.org/10.7289/V5D21VHZ. Accessed 01 11 2024.

Michaelis, A. C., Gershunov, A., Weyant, A., Fish, M. A., Shulgina, T., & Ralph, F. M. (2022). Atmospheric River precipitation enhanced by climate change: A case study of the storm that contributed to California's Oroville Dam crisis. *Earth's Future*, *10*(3), e2021EF002537. https://doi.org/10.1029/2021EF002537

Moragoda, N., & Cohen, S. (2020). Climate-induced trends in global riverine water discharge and suspended sediment dynamics in the 21st century. *Global and Planetary Change*, *191*, 103199. Retrieved from https://doi.org/10.1016/j.gloplacha.2020.103199

Morán-Tejeda, E., López-Moreno, J. I., Stoffel, M., & Beniston, M. (2016). Rain-on-snow events in Switzerland: Recent observations and projections for the 21st century. *Climate Research*, *71*(2), 111–125. https://doi.org/10.3354/cr01435

Mote, P. W., Li, S., Lettenmaier, D. P., Xiao, M., & Engel, R. (2018). Dramatic declines in snowpack in the western US. *NPJ Climate and Atmospheric Science*, *1*(1), 2. https://doi.org/10.1038/s41612-018-0012-1

Musselman, K. N., Lehner, F., Ikeda, K., Clark, M. P., Prein, A. F., Liu, C., et al. (2018). Projected increases and shifts in rain-on-snow flood risk over western North America. *Nature Climate Change*, *8*(9), 808–812. https://doi.org/10.1038/s41558-018-0236-4

Myers, D. T., Ficklin, D. L., & Robeson, S. M. (2023). Hydrologic implications of projected changes in rain-on-snow melt for Great Lakes Basin watersheds. *Hydrology and Earth System Sciences*, *27*(9), 1755–1770. https://doi.org/10.5194/hess-27-1755-2023

NCEI. (2024). National Centers for Environmental Information, Global Historical Climatology Network (GHCN) - daily: README. Retrieved from https://www.ncei.noaa.gov/pub/data/ghcn/daily/readme.txt. Accessed 04 11 2024.

Nielsen, D. M., Pieper, P., Barkhordarian, A., Overduin, P., Ilyina, T., Brovkin, V., et al. (2022). Increase in Arctic coastal erosion and its sensitivity to warming in the twenty-first century. *Nature Climate Change*, *12*(3), 263–270. Retrieved from https://doi.org/10.1038/s41558-022-01281-0

Notarnicola, C. (2020). Hotspots of snow cover changes in global mountain regions over 2000–2018. *Remote Sensing of Environment*, *243*, 111781. https://doi.org/10.1016/j.rse.2020.111781

Ombadi, M., Risser, M. D., Rhoades, A. M., & Varadharajan, C. (2023). A warming-induced reduction in snow fraction amplifies rainfall extremes. *Nature*, *619*(7969), 305–310. Retrieved from https://doi.org/10.1038/s41586-023-06092-7

Pan, C. G., Kirchner, P. B., Kimball, J. S., Kim, Y., & Du, J. (2018). Rain-on-snow events in Alaska, their frequency and distribution from satellite observations. *Environmental Research Letters*, *13*(7), 075004. https://doi.org/10.1088/1748-9326/aac9d3

Pihlainen, S., Zandersen, M., Hyytiäinen, K., Andersen, H. E., Bartosova, A., Gustafs- son, B., & Thodsen, H. (2020). Impacts of changing society and climate on nutrient loading to the Baltic Sea. *Science of the Total Environment*, *731*, 138935. Retrieved from https://doi.org/10.1016/j.scitotenv.2020.138935

Pomeroy, J. W., Fang, X., & Marks, D. G. (2016). The cold rain-on-snow event of June 2013 in the Canadian Rockies — Characteristics and diagnosis. *Hydrological Processes*, *30*(17), 2899–2914. https://doi.org/10.1002/hyp.10905

Pradhanang, S. M., Frei, A., Zion, M., Schneiderman, E. M., Steenhuis, T. S., & Pierson, D. (2013). Rain-on-snow runoff events in New York. *Hydrological Processes*, *27*(21), 3035–3049. https://doi.org/10.1002/hyp.9864

Prein, A. F., & Heymsfield, A. J. (2020). Increased melting level height impacts surface precipitation phase and intensity. *Nature Climate Change*, *10*(8), 771–776. https://doi.org/10.1038/s41558-020-0825-x

Rahimi, R., Ebtehaj, A., Panegrossi, G., Milani, L., Ringerud, S. E., & Turk, F. J. (2022). Vulnerability of passive microwave snowfall retrievals to physical properties of snowpack: A perspective from dense media radiative transfer theory. *IEEE Transactions on Geoscience and Remote Sensing*, *60*, 1–13. Retrieved from https://doi.org/10.1109/TGRS.2022.3184530

Rasiya Koya, S., Kar, K. K., & Roy, T. (2024). Northern Pacific sea-level pressure controls rain-on-snow in North America. *Communications Earth and Environment*, *5*(1), 1–12. https://doi.org/10.1038/s43247-024-01431-6

Rhoades, A. M., Zarzycki, C. M., Hatchett, B. J., Inda-Diaz, H., Rudisill, W., Bass, B., et al. (2024). Anticipating how rain-on-snow events will change through the 21st century: Lessons from the 1997 new year's flood event. *Climate Dynamics*, *62*(9), 8615–8637. Retrieved from https://doi.org/10.1007/s00382-024-07351-7

Roberts-Pierel, B., Kirchner, P., Kilbride, J., & Kennedy, R. (2022). Glacier covered area for the state of Alaska, 1985-2020, version 1. *NSIDC: National Snow and Ice Data Center*. https://doi.org/10.7265/8esq-w553

Ruggiero, P., Komar, P. D., & Allan, J. C. (2010). Increasing wave heights and extreme value projections: The wave climate of the U.S. Pacific Northwest. *Coastal Engineering*, *57*(5), 539–552. https://doi.org/10.1016/j.coastaleng.2009.12.005

Sen, P. K. (1968). Estimates of the regression coefficient based on Kendall's Tau. *Journal of the American Statistical Association*, *63*(324), 1379–1389. https://doi.org/10.1080/01621459.1968.10480934

Siirila-Woodburn, E., Rhoades, A., Hatchett, B., Huning, L., Szinai, J., Tague, C., et al. (2021). A low-to-no snow future and its impacts on water resources in the western United States. *Nature Reviews Earth and Environment*, *2*(11), 800–819. Retrieved from https://doi.org/10.1038/s43017-021-00219-y

Smith, S. G., & Wegmann, K. W. (2018). Precipitation, landsliding, and erosion across the olympic mountains, Washington state, USA. *Geomorphology*, *300*, 141–150. Retrieved from https://doi.org/10.1016/j.geomorph.2017.10.008

Sobota, I., Weckwerth, P., & Grajewski, T. (2020). Rain-On-Snow (ROS) events and their relations to snowpack and ice layer changes on small glaciers in Svalbard, the high Arctic. *Journal of Hydrology*, *590*, 125279. https://doi.org/10.1016/j.jhydrol.2020.125279

Stedinger, J., Vogel, R., & Foufoula-Giorgiou, E. (1993). Frequency analysis of extreme events. In D. Maidment (Ed.), *Handbook of hydrology* (pp. 18.1–18.66). McGraw- Hill.

Stoelinga, M. T., Albright, M. D., & Mass, C. F. (2010). A new look at snowpack trends in the cascade mountains. *Journal of Climate*, *23*(10), 2473–2491. https://doi.org/10.1175/2009JCLI2911.1

Sturm, M., Taras, B., Liston, G. E., Derksen, C., Jonas, T., & Lea, J. (2010). Estimating snow water equivalent using snow depth data and climate classes. *Journal of Hydrometeorology*, *11*(6), 1380–1394. Retrieved from https://doi.org/10.1175/2010JHM1202.1

Tamang, S. K., Ebtehaj, A. M., Prein, A. F., & Heymsfield, A. J. (2020). Linking global changes of snowfall and wet-bulb temperature. *Journal of Climate*, *33*(1), 39–59. Retrieved from https://doi.org/10.1175/JCLI-D-19-0254.1

Tohver, I. M., Hamlet, A. F., & Lee, S.-Y. (2014). Impacts of 21st-century climate change on hydrologic extremes in the pacific northwest region of North America. *JAWRA Journal of the American Water Resources Association*, *50*(6), 1461–1476. Retrieved from https://doi.org/10.1111/jawr.12199

Velásquez, N., Quintero, F., Koya, S. R., Roy, T., & Mantilla, R. (2023). Snow-detonated floods: Assessment of the U.S. midwest march 2019 event. *Journal of Hydrology: Regional Studies*, *47*, 101387. Retrieved from https://doi.org/10.1016/j.ejrh.2023.101387

Wachowicz, L. J., Mote, T. L., & Henderson, G. R. (2020). A rain on snow climatology and temporal analysis for the eastern United States. *Physical Geography*, *41*(1), 54–69. https://doi.org/10.1080/02723646.2019.1629796

Wilcox, R. R. (2010). *Fundamentals of modern statistical methods: Substantially improving power and accuracy*. Springer. https://doi.org/10.1007/978-1-4419-5525-8

Ye, H., Yang, D., & Robinson, D. (2008). Winter rain on snow and its association with air temperature in northern Eurasia. *Hydrological Processes*, *22*(15), 2728–2736. https://doi.org/10.1002/hyp.7094

Zaqout, T., & Andradóttir, H. Ó. (2024). Impacts of climate change on winter flood mechanisms: Spatial variability, trends, and bivariate frequency of rain-on-snow and soil frost. *Journal of Hydrology*, *638*, 131439. https://doi.org/10.1016/j.jhydrol.2024.131439

10.1029/2025GL114775

References From the Supporting Information

Huffman, G. J., Bolvin, D. T., Braithwaite, D., Hsu, K., Joyce, R., Kidd, C., et al. (2019). Algorithm theoretical basis document (ATBD) version 5.2 for NASA global precipitation measurement (GPM) integrated multi-satellite retrievals for GPM (IMERG) (Tech. Rep.). *GPM Project*. Retrieved from https://pmm.nasa.gov/sites/default/files/document_files/IMERG_ATBD_V6.pdf

Ebtehaj, A. M., Bras, R. L., & Foufoula-Georgiou, E. (2015). Shrunken locally linear embedding for passive microwave retrieval of precipitation. *IEEE Transactions on Geoscience and Remote Sensing*, *53*(7), 3720–3736. https://doi.org/10.1109/TGRS.2014.2382436

Ebtehaj, A. M., Bras, R. L., & Foufoula-Georgiou, E. (2016). Evaluation of ShARP passive rainfall retrievals over snow-covered land surfaces and coastal zones. *Journal of Hydrometeorology*, *17*(4), 1409–1424. https://doi.org/10.1175/JHM-D-15-0164.1

Ebtehaj, A. M., & Kummerow, C. D. (2017). Microwave retrievals of terrestrial precipitation over snow-covered surfaces: A lesson from the GPM satellite. *Geophysical Research Letters*, *44*(12), 6154–6162. https://doi.org/10.1002/2017GL073451